

THE SUN: LIGHT DARK MATTER AND STERILE NEUTRINOS

ILÍDIO LOPES^{1, 2} 

¹Centro de Astrofísica e Gravitação - CENTRA,
Departamento de Física, Instituto Superior Técnico - IST, Universidade de Lisboa - UL, Av. Rovisco Pais 1, 1049-001 Lisboa, Portugal and
²Institut d'Astrophysique de Paris, UMR 7095 CNRS, Université Pierre et Marie Curie, 98 bis Boulevard Arago, Paris F-75014, France

(Dated: January 5, 2021)
Draft version January 5, 2021

ABSTRACT

Next-generation experiments allow for the possibility to testing the neutrino flavor oscillation model to very high levels of accuracy. Here, we explore the possibility that the dark matter in the current universe is made of two particles, a sterile neutrino and a very light dark matter particle. By using a 3+1 neutrino flavor oscillation model, we study how such a type of dark matter imprints the solar neutrino fluxes, spectra, and survival probabilities of electron neutrinos. The current solar neutrino measurements allow us to define an upper limit for the ratio of the mass of a light dark matter particle m_ϕ and the Fermi constant G_ϕ , such that G_ϕ/m_ϕ must be smaller than $10^{30} G_F eV^{-1}$ to be in agreement with current solar neutrino data from the Borexino, Sudbury Neutrino Observatory, and Super-Kamiokande detectors. Moreover, for models with a very small Fermi constant, the amplitude of the time variability must be lower than 3% to be consistent with current solar neutrino data. We also found that solar neutrino detectors like Darwin, able to measure neutrino fluxes in the low energy-range with high accuracy, will provide additional constraints to this class of models that complement the ones obtained from the current solar neutrino detectors.

Subject headings: The Sun – Solar neutrino problem – Solar neutrinos – Neutrino oscillations – Neutrino telescopes – Neutrino astronomy

1. INTRODUCTION

The origin of dark matter has been a fundamental problem in physics for almost six decades, during which most of the proposed solutions assumed that a single massive particle that interacts weakly with baryons makes all the dark matter observed in the universe (e.g., Wang et al. 2016). Recently, research has emerged where more sophisticated solutions have been proposed to solve the dark matter problem. One of these is the possibility of the dark matter being a composite of two light particles: a light dark matter (LDM) particle ϕ and a sterile neutrino ν_s .

The existence of such an LDM field can be identified with a dilation field of an extradimensional extension of the Standard Model or/and a CP-violating pseudo-Goldstone boson of a spontaneously broken global symmetry. For some of these models, ϕ couples to the Standard Model fields, and as such it induces periodic time variation in particle masses and couplings. In such theories the gauge invariance suggests that the ϕ should possess an identical coupling constant to charged leptons, in which case scalar interactions with the electrons provide a good opportunity for detection through atomic clocks (e.g., Arvanitaki et al. 2016), accelerometers (e.g., Arvanitaki et al. 2018), and gravitational wave detectors (e.g., Lopes and Silk 2014; Graham et al. 2016).

Similarly, this ϕ field can couple to neutrinos. Once again, these types of interactions generically result in time-varying corrections to the neutrino masses, neutrino mass differences, and mixing angles, which can be searched for in the neutrino flux signals on present and future experimental neutrino detectors (Aharmim et al. 2013; Abe et al. 2016; Borexino Collaboration et al. 2018; Aalbers et al. 2020). If ϕ couples weakly to the neutrinos, over a large range of masses,

it can significantly modify the neutrino oscillations probabilities leading to a distorted survival electron neutrino probability function (Berlin 2016; Krnjaic et al. 2018).

The motivation for such a model comes from the possibility of this composite particle physics model resolving two observational problems:

1. The classical cold dark matter model leads to several inconsistencies with the cosmological observational data, such as the missing satellite problem and the cusp problem (e.g., Primack 2009). Light dark matter resolves such problems if dark matter is totally or partially made of light scalar particles with a mass of the order of $10^{-22} eV$ (Hu et al. 2000; Peebles 2000). In hierarchical models of structure formation, such type of dark matter is able to explain the flatness observed on the profiles of the distribution of gas and stars in halos and filaments (Mocz et al. 2019).
2. Although the standard three neutrino flavor model produces a reasonable good global fit to all the neutrino data (Esteban et al. 2019), there are now many hints that point out to the possibility of the existence of a fourth neutrino. This one does not have any other interaction than gravity and for that reason is known as a sterile neutrino (Diaz et al. 2019). It was found that a flavor oscillation model made of the 3 active neutrinos plus a sterile neutrino could explain some of the observed anomalies found on the Short baseline neutrino oscillation experiments (Giunti et al. 2012, 2013), Liquid Scintillator Neutrino Detector (Aguilar et al. 2001), and MiniBooNE Short-Baseline Neutrino Experiment (MiniBooNE Collaboration et al. 2018), as well as the anomalies related with GALLEX and SAGE solar-neutrino detectors – the so-called Gallium anomalies (Kostensalo et al. 2019). For instance, Kostensalo

et al. (2019) found that the data favour a 3 + 1 neutrino flavor model with $m_4 = 1.1\text{eV}$ and mixing matrix element $U_{e4} = 0.11$.

One possibility to resolve both problems (neutrino anomalies and structure formation) is to consider that dark matter is made of a light scalar field that couples to a sterile neutrino (e.g., Farzan 2019). The interactions of ϕ and ν_s could impede the oscillations in the universe and thereby improve the agreement between the structure formation and cosmological observations (e.g., Dasgupta and Kopp 2014; Hannestad et al. 2014).

If such ϕ and ν_s particles exist today, they were produced abundantly in the early universe. For instance, sterile neutrinos can be produced via mixing with active neutrinos (Dodelson and Widrow 1994), in some scenarios such neutrino production is being enhanced by the oscillations between active and sterile neutrinos (Bezrukov et al. 2019, 2020; de Gouvêa et al. 2020) or by the lepton asymmetry (Shi and Fuller 1999). The production of light dark matter can take many forms, such as vector bosons by parametric resonance production (Dror et al. 2019). For instance, some models predict a sterile neutrino abundance of $\Omega_s^2 h^2 = 0.12 (\sin^2(2\theta_s)/3.5 \times 10^{-9}) (m_{\nu_s}/7\text{keV})$ where m_{ν_s} and θ_s is the sterile neutrino mass and mixing angle (Kusenko 2009). For the light dark matter field some authors obtained $\Omega_\phi^2 = 0.1 (a_o/10^{17} \text{ GeV})^2 (m_a/10^{-22} \text{ eV})^{1/2}$, where a_o is a parameter that relates to the initial misalignment angle of the axion, and m_a is the axion mass (Hui et al. 2017; Niemeyer 2019). Conveniently, we will assume that in the present-day universe the total dark matter abundance is given by

$$\Omega_{\text{DM}} h^2 = \Omega_\phi^2 h^2 + \Omega_{\nu_s}^2 h^2 \quad (1)$$

where the $\Omega_\phi^2 h^2$ and $\Omega_{\nu_s}^2 h^2$ are the total ϕ and ν_s densities in the present universe, respectively. For future reference, we assume that the present-day total dark matter abundance $\Omega_{\text{DM}} h^2 = 0.12$ (Planck Collaboration et al. 2018), and the dark matter density in the solar neighborhood is $\rho_{\text{DM}}^\odot = 0.39 \text{ GeV cm}^{-3}$ (Catena and Ullio 2010).

In this paper, we study the impact that this light dark matter field has in the 3+1 neutrino flavor model. Specifically, we discuss how the light dark matter field modifies the neutrino flavor oscillations, and by using the current sets of solar neutrino data, we also put constraints in the parameters of such models and make predictions for the future neutrino experiments.

The article is organized as follows. In section 2, we discuss how the light dark matter drives the 3+1 neutrino flavor oscillations. In section 3, we present the neutrino flavor oscillation model in the presence of a cosmic light dark matter field. In section 4, we compute the survival electron neutrino probabilities for the electron neutrinos produced in the proton-proton (PP) chain and carbon-nitrogen-oxygen (CNO) cycle solar nuclear reactions. In section 5, we discuss the results in relation to current experiments and future ones. Finally, in section 6, we present the conclusion and a summary of our results.

If not stated otherwise, we work in natural units in which $c = \hbar = 1$. In these units all quantities are measured

in GeV, and we make use of the conversion rules $1\text{m} = 5.068 \times 10^{15} \text{ GeV}^{-1}$, $1\text{kg} = 5.610 \times 10^{26} \text{ GeV}$ and $1\text{sec} = 1.519 \times 10^{24} \text{ GeV}^{-1}$.

2. LIGHT DARK MATTER AND STERILE NEUTRINOS IN THE UNIVERSE

We assume that in the present universe, the dark matter is composed of two fundamental particles: a light scalar boson ϕ and sterile neutrinos ν_s , where m_ϕ and m_{ν_s} are their respective masses (Hannestad et al. 2014). The LDM field ϕ couples with the active neutrinos and the sterile neutrino by a Yukawa interaction $g_\phi \phi \nu_s \nu_s$ where g_ϕ is a dimensionless coupling (Farzan 2019). To illustrate this effect, consider an LDM scalar ϕ with a Yukawa coupling to active neutrinos. Then the relevant part of the Lagrangian reads

$$\mathcal{L} \supset - (m_\nu + g_\phi \phi) \nu \nu + \text{H.c.}, \quad (2)$$

where for convenience of representation the flavor indices have been suppressed. We also assume that the dimensionless coupling is very small ($g \ll 1$). From the Euler-Lagrange equations of ν and ϕ , it is possible to show that the effect of ϕ on the propagation of the neutrino is equivalent to changing the neutrino mass from m_ν to $m_\nu + \delta m_\nu$. As we will see later, this δm_ν perturbation will induce time variations in the mass-squared differences and mixing angles of all neutrino flavors through ϕ . In principle the Yukawa couplings can have any structure in the neutrino flavor space. In this work, we will focus on two convenient scenarios of great interest to neutrino detectors: mass-square differences and mixing angles (e.g., Ding and Feruglio 2020). Moreover, we will also assume that $\delta m_\nu = g_\phi \phi$ (e.g., Smirnov and Xu 2019).

2.1. Dark Matter Time-dependent Variation

The hypothesis that dark matter in the local universe is made of very light particles leads to the following description: the LDM field ϕ in the dark matter halo of the Milky Way is represented by a group of plane waves with frequency ω_ϕ , such that $\omega_\phi = m_\phi (1 + v_\phi^2/2)$ where v_ϕ is the virial velocity of the particles in the dark halo. A population of such light particles will smooth inhomogeneities in the dark matter distribution on scales smaller than the de Broglie wavelength λ_{dB} of these LDM particles. For any particle, we compute λ_{dB} using the relation $\lambda_{\text{dB}} = 1.24 \times 10^{22} (10^{-23} \text{ eV}/m_\phi) (10^{-3}/v_\phi) \text{ cm}$.

We notice that the kinetic term on ω_ϕ is neglected once the virial velocity $v_\phi \sim 10^{-3}$ is very small (e.g., Blas et al. 2017). Therefore, we dropped the corrections related with v_ϕ for the equation 2. Accordingly, the general form of this LDM field reads

$$\phi(\vec{r}, t) = \phi_o \cos(m_\phi t + \epsilon_o) \approx \phi_o \cos(m_\phi t), \quad (3)$$

where ϕ_o and $\epsilon_o = \vec{v}_\phi \cdot \vec{r}$ are the amplitude and phase of the wave $\phi(t)$, respectively. In this work we consider $\epsilon_o \approx 0$. Moreover, the energy momentum of a free massive oscillating field has a density given by $\rho_\phi = \phi_o m_\phi/2$ and a pressure given by $p_\phi = -\rho_\phi \cos(2m_\phi t)$. Although formally ρ_ϕ has an oscillating part proportional to $\phi(t)$, because this component is very small we neglected its contribution in this analysis (Khmelnitsky and Rubakov 2014).

The quantity ϕ_o is a slowly varying function of the position. Conveniently, the amplitude of $\phi(t)$ can be written

as $\phi_o = \sqrt{2\rho_\phi(r)}/m_\phi$ where $\rho_\phi(r) = \rho_{\text{DM}}^\odot (\Omega_\phi/\Omega_{\text{DM}})$ is the fraction of dark matter density in ϕ particles at the space-time coordinate \vec{r} . Accordingly, the Sun immersed in this light dark matter halo will experience a periodic perturbation due to the action of the $\phi(\vec{r}, t)$, which by the presence of a Yukawa coupling g_ϕ will exert a temporal variation on the propagation of all neutrinos. We estimate the dark matter density number n_ϕ in the solar neighborhood as follows: if we consider that the main contribution arises from a single dark matter particle with mass m_ϕ , then the relevant density in our case will take the value $n_\phi = \rho_\phi/m_\phi$. If we assume that all dark matter is made of ϕ bosons, we have $\rho_\phi = \rho_{\text{DM}}^\odot = 0.39 \text{ GeV cm}^{-3}$ (Catena and Ullio 2010) and $m_\phi = 10^{-22} \text{ eV}$ then $n_\phi = 3.9 \times 10^{30} \text{ cm}^{-3}$ (particles per centimeter cubed). This value is only 2 orders of magnitude smaller than the density of electrons in the Sun's core, $n_e \sim 6 \cdot 10^{31} \text{ cm}^{-3}$ (Lopes and Turck-Chièze 2013). Since these particles are very light, we assume that there is no accretion of these particles in the Sun's core during its evolution in the main sequence until the present age.

2.2. Neutrino Time-dependent Dark-matter-induced Oscillations

In the presence of the LDM field ϕ , the neutrino mass m_ν , according to equation 2 (Ding and Feruglio 2020), will receive a contribution $\delta m_\nu = g_\phi \phi$, such that from equation 3, we obtain

$$\frac{\delta m_\nu}{m_\nu} = \epsilon_\phi \cos(m_\phi t), \quad (4)$$

where ϵ_ϕ is the amplitude

$$\epsilon_\phi = \frac{g_\phi \sqrt{2\rho_\phi}}{m_\phi m_\nu} = \frac{g_\phi \sqrt{2\rho_{\text{DM}}^\odot}}{m_\phi m_\nu} \left(\frac{\Omega_\phi}{\Omega_{\text{DM}}} \right)^{1/2}. \quad (5)$$

If not stated otherwise, we will assume that all dark matter in the present universe is made of only LDM particles such that $\Omega_\phi = \Omega_{\text{DM}}$. We observe that ϵ_ϕ is a relevant factor even if ϕ is a small fraction of the dark matter halo. In particular, ϕ will affect the oscillation parameters of all neutrino flavors, including the sterile sterline neutrinos. If we only take into account the first order perturbation, thus, the neutrino mass-squared difference can be written as

$$\Delta m_{ij}^2(t) = m_i^2 - m_j^2 \approx \Delta m_{ij,o}^2 [1 + 2\epsilon_\phi \cos(m_\phi t)] \quad (6)$$

where $\Delta m_{ij,o}^2$ is the standard (undistorted) value and $\Delta m^2(t)$ evolves through $\phi(t)$ (see Equation 3), with an amplitude ϵ_ϕ (see Equation 5), and a frequency m_ϕ . The mass-squared difference Δm_{ij}^2 between neutrinos of different flavors follows the usual convection (e.g., Lopes 2017) such that $\Delta m_{i1}^2 = m_i^2 - m_1^2$ ($i=2, 3, 4$). In particular for the sterile neutrino, we have $\Delta m_{41}^2 = m_4^2 - m_1^2$ where m_4 is the mass of the sterile neutrino. Similarly, the mixing angles variation is written as

$$\theta_{ij}(t) \approx \theta_{ij,o} + \epsilon_\phi \cos(m_\phi t), \quad (7)$$

where $\theta_{ij,o}$ is the standard (undistorted) mixing angle. The indexes i and j in θ_{ij} follow a convention identical but not equal for the mass-squared differences (see Lopes 2018a, and references therein). Therefore, as first suggested by Krnjaic et

al. (2018), the LDM $\phi(t)$ impacts the neutrino flavor oscillations through the modified expressions for the mass-squared differences (Equation 6) and mixing angles (Equation 7).

3. LIGHT DARK MATTER AND THE STERILE NEUTRINO MODEL

In the following section, we consider a 3+1 neutrino flavor oscillation model to describe the propagation of active neutrinos (ν_e, ν_τ, ν_μ) plus a sterile neutrino ν_s through the solar plasma. Following the usual notation ($\nu_e, \nu_\tau, \nu_\mu, \nu_s$) corresponds to the neutrino flavors, ($\nu_1, \nu_2, \nu_3, \nu_4$) are the mass neutrino eigenstates, and (m_1, m_2, m_3, m_4) are the neutrino masses. The evolution of neutrinos propagating in matter is described by the see

$$i \frac{d\Psi}{dr} = \mathcal{H}\Psi = \frac{1}{2E} (\mathbf{U}M^2\mathbf{U}^\dagger + 2E\mathcal{V}) \Psi, \quad (8)$$

where \mathcal{H} is the Hamiltonian and $\Psi = (\nu_e, \nu_\tau, \nu_\mu, \nu_s)^\top$. M^2 is a neutrino mass matrix, \mathbf{U} is a (4×4) unitary matrix describing the mixing of neutrinos and \mathcal{V} is the diagonal matrix of Wolfenstein potentials (Kuo and Pantaleone 1989). M^2 is defined as $M^2 = \text{diag}\{0, \Delta m_{21}^2, \Delta m_{31}^2, \Delta m_{41}^2\}$. The first term of the Hamiltonian describes the neutrino propagation through vacuum and the second term incorporates the matter effects or Mikheyev-Smirnov-Wolfenstein (MSW) effects (Wolfenstein 1978; Mikheyev and Smirnov 1985). In general, the Hamiltonian \mathcal{H} that drives the evolution of neutrino flavor must include the Wolfenstein potentials related with $\phi(t)$ (Brdar et al. 2018).

In most studies of three-neutrino flavor models, the authors are solely interested in the modulation coming from the square mass differences $\Delta m_{ij}^2(t)$ (by Equation 6) and mixing angles $\theta_{ij}(t)$ (by Equation 7). For that reason, all neutrinos are assumed to couple $\phi(t)$. As a consequence, their contribution to \mathcal{V} cancels out. Hence, it is correct to neglect the contribution of $\phi(t)$ to the Wolfenstein potential (Dev et al. 2020). Nevertheless, here in this 3+1 neutrino flavor model, as we will discuss later, we include the contribution of $\phi(t)$ in \mathcal{V} .

This 3+1 neutrino flavor model with dark matter is identical to the standard (undistorted) three-neutrino flavor model (see Equation 8). However, in this model we included a sterile neutrino, and the Wolfenstein potentials in \mathcal{V} are modified to take into account the new LDM field ϕ (Miranda et al. 2015).

3.1. Neutrino Matter-induced Oscillations

In the standard three-neutrino flavor model¹, the matter potential \mathcal{V} takes into account the interaction of active neutrinos (ν_e, ν_μ, ν_τ) with the ordinary fermions of the solar plasma, for which the $\mathcal{V} = \text{diag}\{V_{cc} + V_{nc}, V_{nc}, V_{nc}\}$ where V_{cc} corresponds to the weak charged current (cc) that takes into account the forward scattering of ν_e with electrons, and V_{nc} is the weak neutral current (nc) that corresponds to the scattering of the active neutrinos with the ordinary fermions of the solar plasma (e.g., Xing 2020). V_{nc} can be expressed as $V_{nc} = V_{nc}^e + V_{nc}^p + V_{nc}^n$ where V_{nc}^j with $j = e, p, n$ are the contributions coming from electrons, protons, and neutrons, respectively. However due to the electrical neutrality of the solar plasma, the contribution of V_{nc}^e and V_{nc}^p canceled out

¹ In this model, the intermediate particle is a heavy boson, specifically the Z or W^\pm bosons.

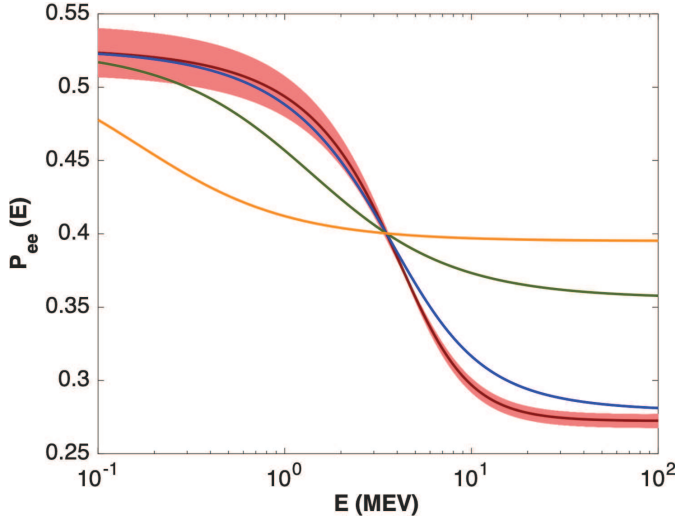


FIG. 1.— The survival probability electron neutrinos $P_{ee}(E, \phi)$ and $\langle P_{ee}(E) \rangle$ in a 3+1 neutrino flavor oscillation model in which neutrino couple to the light dark matter field ϕ with fixed value of m_ϕ and ϵ_ϕ (see main text). The figure shows $\langle P_{ee}(E) \rangle$ (with $\epsilon_\phi \approx 0\%$) for the following LDM models with G_ϕ/m_ϕ ratios: $10^{29} G_F eV^{-1}$ (blue curve), $10^{30} G_F eV^{-1}$ (green curve), $10^{31} G_F eV^{-1}$ (orange curve). The figure also shows a model with $G_\phi \approx 0$ (red curve) and an ensemble of $P_{ee}(E, \phi)$ corresponding to different time-varying mass-square differences and angles for $\epsilon_\phi = 1.5\%$ (pink band). See main text for details.

such that $V_{nc} = V_{nc}^n$. Accordingly, $V_{cc} = \sqrt{2}G_F n_e(r)$ and $V_{nc} = V_{nc}^n = G_F/\sqrt{2} n_n(r)$. Here G_F is the Fermi constant and $n_e(r)$ and $n_n(r)$ are the number density of electrons and neutrons inside the Sun. Nevertheless, since V_{nc} is an universal term for all active neutrino flavors, and as such does not change the flavor oscillations pattern, conveniently we write $\mathcal{V} = \text{diag}\{V_{cc} + 0, 0, 0\}$. Now, the inclusion of sterile neutrinos in the neutrino flavor model alters \mathcal{V} (from Equation 8) by incorporating a new degree of freedom, as a consequence $\mathcal{V} = \text{diag}\{V_{cc} + V_{nc}, V_{nc}, V_{nc}, 0\}$ (e.g., [Giunti and Li 2009](#); [Maltoni and Smirnov 2016](#); [Xing 2020](#)).

Finally, in our 3+1 neutrino flavor model, we include the interaction of active and sterile neutrinos with the dark matter field ϕ by means of an intermediate heavy boson I^2 . These interactions result from the forward scattering of these neutrinos through the LDM field ϕ , thus $\mathcal{V} = \text{diag}\{V_{cc} + V_{nc} + V_{\nu_e\phi}, V_{nc} + V_{\nu_\mu\phi}, V_{nc} + V_{\nu_\tau\phi}, V_{nc} + V_{\nu_s\phi}\}$, where $V_{\nu_i\phi}$ (with $\nu_i = \nu_e, \nu_\mu, \nu_\tau, \nu_s$) relates to the neutrino ν_i . This \mathcal{V} corresponds to a generalization of the Wolfenstein potentials found in the literature, for which most neutrino flavor models only take into account the scattering of the sterile neutrinos on heavy dark matter ([Capozzi et al. 2017](#); [Lopes 2018a](#); [Lopes and Silk 2019](#)).

In our model, we opt to assume that all active neutrinos experience the same interaction with the LDM field ϕ , such that their dark matter potentials are the same, such that $V_{\nu_j\phi} = V_{\nu_a\phi}$ (with $j = e, \mu, \tau$), it follows $\mathcal{V} = \text{diag}\{V_{cc} + V_{nc} + V_{\nu_a\phi}, V_{nc} + V_{\nu_a\phi}, V_{nc} + V_{\nu_a\phi}, V_{nc} + V_{\nu_s\phi}\}$. Now, if we subtract the common term $V_{nc} + V_{\nu_a\phi}$ to the diagonal matrix \mathcal{V} , the latter takes the simple form: $\mathcal{V} = \text{diag}\{V_{cc}, 0, 0, V_{\nu_s\phi} - V_{\nu_a\phi} - V_{nc}\}$.

The potential $V_{\nu_i\phi}$ (with $i = a, s$) is given by $V_{\nu_i\phi} = G_{\nu_i\phi} n_\phi$ where $G_{\nu_i\phi}$ is the equivalent of the Fermi con-

² We assume the boson I has a mass m_I identical to Z and W^\pm bosons.

stant and n_ϕ is the distribution of dark matter inside the Sun ([Smirnov and Xu 2019](#)). Equally, $V_{\nu_i\phi}$ relates directly with the local density of dark matter ρ_{DM}^\odot by the expression: $V_{\nu_s\phi} = (G_{\nu_s\phi}/m_\phi) (\rho_{DM}^\odot \Omega_\phi / \Omega_{DM})$, where we assume the ratio $G_{\nu_s\phi}/m_\phi$ is a free parameter of the LDM model. The generalized Fermi constant is defined as $G_{\nu_i\phi} = g_{\nu_i} g_\phi / m_I^2$ where g_{ν_i} represents the coupling constant of the corresponding neutrino ν_i , and m_I is the mass of the intermediate boson I ([Miranda et al. 2015](#)). This expression for the potential $V_{\nu_i\phi}$ is valid since we assume that $m_I^{-1} \ll R_\odot$ where R_\odot is the solar radius³ ([Smirnov and Xu 2019](#)). In general, we could expect that the contribution of $\phi(t)$ to $V_{\nu_i\phi}$ could lead to a time-dependent relation, however, as discussed previously (in section 2.1) and mentioned for the first time by [Khmelnitsky and Rubakov \(2014\)](#), this is because the oscillatory component on the local density relates with v_ϕ^2 . This term is minimal, and therefore we neglected it.

In this preliminary study, without loss of generality, we choose to simplify \mathcal{V} further: since the term $V_{\nu_s\phi} - V_{\nu_a\phi} - V_{nc}$ has two Wolfenstein potentials ($V_{\nu_a\phi}$ and $V_{\nu_s\phi}$) that effectively correspond to two new degrees of freedom, both of these have an identical impact on the neutrino flavor oscillation model. We choose to simplify the model by assuming that $V_{\nu_a\phi}$ is much smaller than V_{nc} . Consequently, \mathcal{V} takes the simplified form: $\mathcal{V} \approx \text{diag}\{V_{cc}, 0, 0, V_{\nu_s\phi} - V_{nc}\}$. For reference, we note that in the Sun's core V_{nc} is always smaller than V_{cc} , once n_e is more than twice as larger as n_n (e.g. [Lopes 2018b](#)). This potential is identical to others found in the literature, for instance in [Capozzi et al. \(2017\)](#) and [Lopes \(2018a\)](#). Therefore, the matter potential $V_{\nu_s\phi}$ reads $V_{\nu_s\phi} = G_{\nu_s\phi} n_\phi$ where for convenience of analysis, we choose to define the generalized Fermi constant as $G_{\nu_s\phi} = 4\sqrt{2}G_\phi G_F$ where G_ϕ is our free parameter. Since these dark matter particles have a mass much smaller than 4 GeV, the solar plasma conditions do not allow the accretion of dark matter by the Sun (e.g., [Lopes and Lopes 2019](#)), therefore we will assume that the distribution of dark matter inside the star is equal to the value measured for the solar neighborhood n_ϕ (see section 2.1).

3.2. Neutrino Flavor Oscillation Model and the Survival Probability of Electron Neutrinos

If we adopt as reference the current experimental set of parameters for the active neutrinos (e.g., [Esteban et al. 2019](#)), the propagation neutrinos in the solar interior are completely adiabatic. The same is valid for the 3+1 neutrino flavor oscillation model coupled to an LDM field ϕ considered in this study. Conveniently, the propagation of neutrinos away from resonances is well represented by a two neutrino flavor oscillation model. The motivation for such approximation can be found in [Lopes \(2018b\)](#) and references therein. In such a case, the electron neutrino flavor oscillation is dominated by the (ν_1, ν_2) mass eigenstates and is only slightly affected by the decoupled (ν_3, ν_4) eigenstates, since the associated mixing angles for the latter pair are very small ([Kuo and Pantaleone 1986](#)). Moreover, ν_3 and ν_4 evolve independent of each other and are completely independent of the doublet (ν_1, ν_2) . In this limit, as proposed by several authors (e.g. [Palazzo 2011](#);

³ As an example, if we consider $m_I \approx m_Z \approx 90 \text{ GeV}$ where m_Z is the mass of the Z boson, then the propagation of neutrinos (like of the neutral current) verifies the condition $m_I^{-1} \ll R_\odot$.

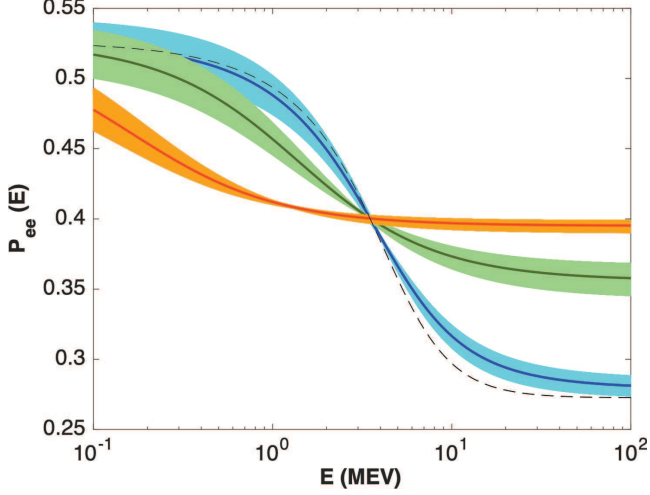


FIG. 2.— The survival probability electron neutrinos $P_{ee}(E, \phi)$ and the corresponding $\langle P_{ee}(E) \rangle$ for some of the models shown in figure 1 for which $\epsilon_\phi = 1.5\%$: $G_\phi = 10^{20} G_F$ (blue band and dark blue curve), $G_\phi = 10^{21} G_F$ (green band and dark green curve) and $G_\phi = 10^{22} G_F$ (orange band and dark red curve). The figure also shows $\langle P_{ee}(E) \rangle$ for the 3+1 model with no time dependence ($G_\chi \approx 0$) and $\epsilon_\phi \approx 0$) as a thin dashed black curve. The latter curve corresponds to the red curve in figure 1.

Blennow and Smirnov 2013), the split of the 3+1 neutrino flavor model into a dominant two neutrino flavor model (ν_e, ν_μ) with additional corrections for ν_τ and ν_s significantly simplified the calculation and allowed us to obtain an analytical solution (e.g., Kuo and Pantaleone 1989).

Among the many expressions available in the literature to compute the survival probability of electron neutrinos P_e (e.g., Lunardini and Smirnov 2000; Miranda et al. 2015) in a 3+1 neutrino flavor model developed in the approximate scenario of a two-flavor neutrino model (e.g., Kuo and Pantaleone 1989), we opted to choose the expression obtained by Capozzi et al. (2017) for the case in which $V_{cc}E/\Delta m_{31}^2 \ll 1$ (and $s_{34} = 0$) which has a better numerical accuracy than others. In that case the survival probability of electron neutrinos, i.e., $P_e \equiv P(\nu_e \rightarrow \nu_e)$, reads

$$P_{ee}(E, \phi) = s_{13}^4 + c_{13}^4 c_{24}^4 c_{14}^4 + a_m + b_m, \quad (9)$$

where $c_{ij} = \cos \theta_{ij}$ and $s_{ij} = \sin \theta_{ij}$. The functions a_m and b_m are dependent on the internal structure of the Sun and are given by the expressions:

$$a_m = C_1 (s_m c_{14} - c_m s_{14} s_{24})^2 \quad (10)$$

and

$$b_m = C_2 (c_m c_{14} + s_m s_{14} s_{24})^2 \quad (11)$$

where $c_m = \cos \theta_m$, $s_m = \sin \theta_m$, $C_1 = c_{13}^4 (c_{14} s_{12} - c_{12} s_{14} s_{24})^2$ and $C_2 = c_{13}^4 (c_{12} c_{14} + s_{12} s_{14} s_{24})^2$. The angle θ_m is obtained for the present-day Sun (i.e., the standard solar model, see details of this model in Lopes and Silk 2013) using the expression (Capozzi et al. 2017): $\cos(2\theta_m) = \mathcal{M}_x (\mathcal{M}_y^2 + \mathcal{M}_x^2)^{-1/2}$, where $\mathcal{M}_x \equiv \cos(2\theta_{12}) - \eta_\nu V_x$ and $\mathcal{M}_y \equiv |\sin(2\theta_{12}) + \eta_\nu V_y|$. η_ν is the ratio of the energy of the neutrino E in relation to Δm_{21}^2 given by $\eta_\nu(E) = 4E/\Delta m_{21}^2$. The functions V_x and V_y are given by

$$V_x = \frac{1}{2} [V_{cc} c_{13}^2 (c_{14}^2 - s_{14}^2 s_{24}^2) + V_s (s_{14}^2 - c_{14}^2 s_{24}^2)], \quad (12)$$

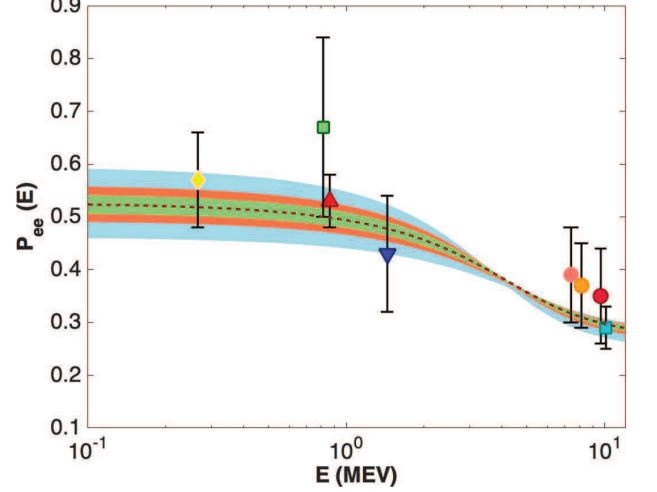


FIG. 3.— The survival probability of the electron neutrinos for several solar nuclear reactions: pp (yellow diamond), ${}^7\text{Be}e$ (green square), ${}^7\text{Be}$ (red upward triangle), pep (blue downward triangle) and ${}^8\text{B}$ HER (salmon circle), ${}^8\text{B}$ HER-I (orange circle), ${}^8\text{B}$ HER-II (magenta circle) and ${}^8\text{B}$ (cyan square). The diamond, triangle, and circles points use data from the Borexino (Borexino Collaboration et al. 2020; Agostini et al. 2019; Borexino Collaboration et al. 2018; Bellini et al. 2010) and the two square data points correspond to data obtained from SNO (Aharmim et al. 2013) and Super-Kamiokande (Abe et al. 2016; Cravens et al. 2008) detectors. Each color band corresponds to an ensemble of $P_{ee}(E, \phi)$ (Equation 9) in a 3+1 neutrino model with $G_\phi \approx 0$ and $\epsilon_\phi \approx 0$ (dashed curve), 1.5% (green), 3.0% (orange) and 6.0% (light blue). These survival probabilities are computed using an high-Z SSM (see the main text) and the experimental values from the different neutrino experiments.

$$V_y = (V_s - V_{cc} c_{13}^2) c_{14} s_{14} s_{24} \quad (13)$$

and

$$V_s = V_{\nu_s \phi} - V_{nc}. \quad (14)$$

3.3. Light Dark Matter Impact on Solar Neutrinos

The survival probability of electron neutrinos (Equation 9) is a time-dependent function through equations (6), (7) and (3). Conveniently we define an effective oscillation probability $\langle P_{ee}(E) \rangle$ that corresponds to an ensemble average of all the $P_{ee}(E, \phi)$ (Equation 9), as such

$$\langle P_{ee}(E) \rangle = \int_0^{\tau_\phi} P_{ee}(E, \phi) \frac{dt}{\tau_\phi}, \quad (15)$$

where $\tau_\phi = 2\pi/m_\phi$ is the period of the LDM field $\phi(t)$.

The ability of a solar neutrino detector to measure the impact of the time-dependent LDM field $\phi(t)$ on the survival probability $P_{ee}(E, \phi)$ (Equation 9) depends on three characteristic time scales: the neutrino flight time τ_ν , the time between two consecutive neutrino detections τ_{ev} , and the total run time of the experiment τ_{ex} . The neutrino flight time is proportional to the Earth-Sun distance d_\oplus such that $\tau_\nu = d_\oplus/c \approx 8.2$ min where c is the speed of light. The number of events measured by a detector varies strongly from one to another.

The next generation of experiments will have τ_{ev} much larger than the pioneer Homestake experiment that only detects a few events per year (Bahcall and Davis 1976). The forthcoming Jiangmen Underground Neutrino Observatory (JUNO; Adam et al. 2015) experiment expects to measure a few tens

of neutrinos per day (for instance 200 events per day or $\tau_{ev} \approx 7$ min). The total experimental run time for most solar neutrino detectors is of the order of a few decades (for instance $\tau_{ex} \approx 10$ yr), and future experiments will also have significant running times. Hence for all models considered in this study, we assume that solar neutrino detectors will run for long periods and will collect a large number of events, therefore we assume that τ_{ev} and τ_{ex} have sufficient small and large values, respectively.

In such conditions, the solar neutrino spectra time modulation by $\phi(t)$ depends on the period τ_ϕ of the LDM field in comparison to the flight time of solar neutrinos τ_ν . Since these neutrinos have a $\tau_\nu \approx 8.2$ min, it is possible to find the value of m_ϕ for which $\tau_\nu = \tau_\phi$ which occurs for $m_{\phi,c} = 8.3 \cdot 10^{-18}$ eV. Accordingly, we can define two regimes for the time modulation of survival probability of electron neutrinos :

1. For $\tau_\phi \geq \tau_\nu$ (low-frequency regime or low LDM mass), the time modulation of $P_{ee}(E, \phi)$ occurs when the period of $\phi(t)$ is larger than τ_ν . In this case a temporal variation of the neutrino signal may be observed. This corresponds to a LDM field with a mass such that $m_\phi \leq m_{\phi,c}$. Therefore, the LDM field can induce an observable time variation in neutrino oscillation measurements as periodicity in the solar neutrino fluxes (Berlin 2016). Obviously, if τ_ϕ becomes very large, the modulation of $P_{ee}(E, \phi)$ becomes indistinguishable from the standard scenario (undistorted case), since the running time of the experiment is not sufficient to observe this phenomena. Nevertheless, in our study, the LDM field has always an $m_\phi \geq 10^{-23}$ eV or a period $\tau_\phi \geq 13$ yr. Therefore, it is always possible to probe such a model with current experimental running times.
2. For $\tau_\phi \leq \tau_\nu$ (high-frequency regime or high LDM mass), the change of $P_{ee}(E, \phi)$ due to $\phi(t)$ is too fast to be observed as a modulating signal like in the previous case. This regime occurs for LDM fields with a mass such that $m_\phi \geq m_{\phi,c}$. Nevertheless, the time average of the ensemble of oscillation probability $P_{ee}(E, \phi)$ can be distorted in such a regime, hence the effect can be detected as $\langle P_{ee}(E) \rangle$ which will deviate from the standard scenario (Krnjaic et al. 2018). The net effect of averaging over time induces a shift in the observed values of $P_{ee}(E, \phi)$ relative to its undistorted value.

Therefore, we can expect to study both regimes in a quite reasonable range of LDM masses using data from the present and future solar neutrino experiments. In fact, some of the current solar neutrino detectors have already large statistics and high event rates that we can use to look for time modulations in solar neutrinos. Some of these neutrino collaborations have already searched for regular phenomena with periods varying from 10 minutes to 10 yr (e.g., Yoo et al. 2003; Aharmim et al. 2010).

In this work, we will study models that will fall in these two regimes of time modulation. Therefore to satisfy the conditions mentioned above, we decided to analyze the impact of the LDM field in solar neutrino fluxes for $\phi(t)$ with a period τ_ϕ varying from 4 μ s to 13 yr or equivalently with a m_ϕ varying from 10^{-9} eV to 10^{-23} eV, which is a range possible to be scanned by future detectors like Deep Underground

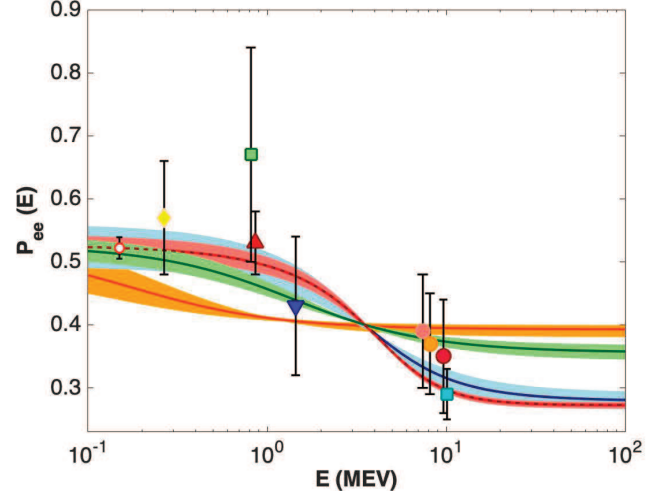


FIG. 4.— The survival probability of the electron neutrinos for several LDM models (see the main text and caption of figure 3 and 2 for details). The LDM models are identical to the ones presented in Figure 2, with the following changes: (i) $G_\phi = 0$ and $\epsilon_\phi = 1.5\%$ (red band); (ii) $G_\phi = 10^{20} G_F$ and $\epsilon_\phi = 3.0\%$ (light-blue band); (iii) $G_\phi = 10^{21} G_F$ and $\epsilon_\phi = 1.5\%$ (green band); (iv) $G_\phi = 10^{22} G_F$ and $\epsilon_\phi = 3.0\%$ (orange band). The data points correspond to the same ones displayed in figure 3. However, the data with the lowest energy corresponds to the expected precision to be attained by the Darwin experiment in measuring $P_{ee} \pm \Delta P_{ee}$, for which ΔP_{ee} could be as low as $\Delta P_{ee} = 0.017$ (Aalbers et al. 2020). The continuous dashed curve corresponds to a 3+1 neutrino model with $G_\phi \approx 0$ and $\epsilon = 0\%$.

Neutrino Experiment (DUNE Collaboration et al. 2015) and JUNO (An et al. 2016).

4. LIGHT DARK MATTER IMPACT ON ELECTRON NEUTRINO SPECTRA

Inside the Sun, the flux variation of neutrinos with different flavors due to matter (including LDM) is strongly dependent of the local distributions of electrons and neutrons, but also on the population of dark matter particles in the solar neighbourhood. This new flavor mechanism (sterile neutrinos and LDM field ϕ) affects all electron neutrinos produced in the Sun's core. A detailed discussion about the neutrino sources inside the Sun, and their specific solar properties, can be found in Lopes (2013, 2017). The average survival probability of electron neutrinos for each nuclear reaction in the solar interior, i.e., $P_{e,i}(E, \phi)$ is computed by

$$P_{e,e,i}(E, \phi) = C_i \int_0^{R_\odot} P_e(E, \phi, r) S_i(r) 4\pi\rho(r)r^2 dr, \quad (16)$$

where $C_i \left(= \left[\int_0^{R_\odot} S_i(r) 4\pi\rho(r)r^2 dr \right]^{-1} \right)$ is a normalization constant and $S_i(r)$ is the electron neutrino emission function for the i solar nuclear reaction. i corresponds to the following solar neutrino sources (from the PP chain and CNO cycle nuclear reactions): pp, pep, 8B , 7Be , ^{13}N , ^{15}O and ^{17}F .

Moreover, since the survival probabilities $P_{e,e,i}(E, \phi)$ (Equation 16) are time dependent through ϕ , these quantities also vary with time. Therefore, the oscillation probability $\langle P_{ee}(E) \rangle$ (Equation 15) is generalized for each specific nuclear reaction i :

$$\langle P_{e,e,i}(E) \rangle = \int_0^{\tau_\phi} P_{e,i}(E, \phi) \frac{dt}{\tau_\phi}. \quad (17)$$

The LDM field ϕ can lead to different temporal imprints on

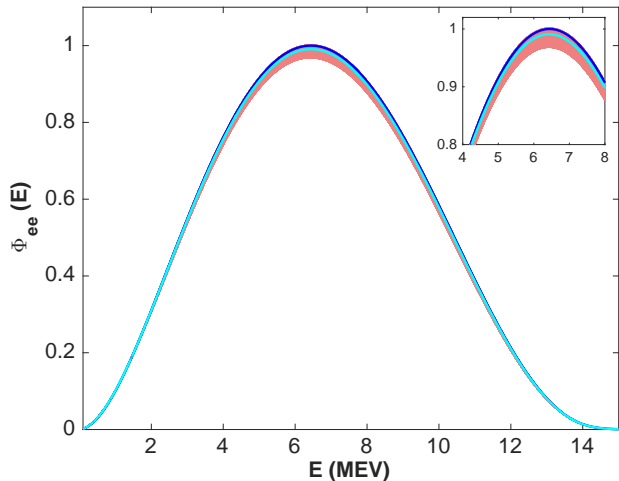


FIG. 5.— The ^8B solar electron neutrino spectra measured on Earth detectors. The blue curve corresponds to the standard (undistorted) neutrino spectra, the cyan curve to the averaged (distorted) electron spectra, and the red band corresponds to the ensemble of spectra related with the time-dependent flavor parameters. This LDM model has a $G_\phi \approx 0$ and an $\epsilon_\phi = 3.0\%$. In the calculation of the ^8B spectrum we use a high-Z SSM (see the main text).

the neutrino oscillation measurements. The specific impact depends on the mass of the LDM particle. In the following, we compute the spectra of neutrinos from any specific nuclear reaction that we know to be essentially independent of the properties surrounding solar plasma. Since in the 3+1 neutrino flavor model new processes exist to change the survival probability of electron neutrinos, this will modify the solar neutrino spectra measured on Earth. These new processes will alter the conversion rates of ν_e to other flavors (ν_μ , ν_τ and ν_s) and vice versa. Accordingly, the electron neutrino spectrum of the nuclear reaction i inside the core is defined as Φ_i , and $\Phi_{i,\odot}$ is the electron neutrino spectrum arriving on Earth (Lopes 2018b) such that:

$$\Phi_{i,\odot}(E) = P_{ee,i}(E, \phi)\Phi_i(E) \quad (18)$$

where $P_{ee,i}(E)$ is the average survival probability of electron neutrinos for reactions in the solar interior as given by equation 16. Equally if we take the time average of equation 18, we obtain the following averaged spectrum for each nuclear reaction i :

$$\Phi_{i,\odot}(E) = \langle P_{ee,i}(E) \rangle \Phi_i(E), \quad (19)$$

where $\langle P_{ee,i}(E) \rangle$ is the average survival probability of electron neutrinos as given by equation 17.

5. THE SUN: LIGHT DARK MATTER AND STERILE NEUTRINOS

Here, we will study the impact of the theoretical model presented in the previous sections, specifically we compute the survival probability of electron neutrinos (as given by equations (9), (15), (16) and (17)) in the case of a standard solar model with low-Z (e.g., Lopes and Silk 2013; Capelo and Lopes 2020).

In the parameterization for the 3+1 neutrino flavor oscillation model, we opt to adopt the recent values obtained in the data analysis of the standard three-neutrino flavor oscillation model obtained by de Salas et al. (2020), and for the sterile neutrino additional fiducial parameters we used the values obtained by Gariazzo et al. (2015). Accordingly, for a parameterisation with a normal ordering of neutrino masses, the

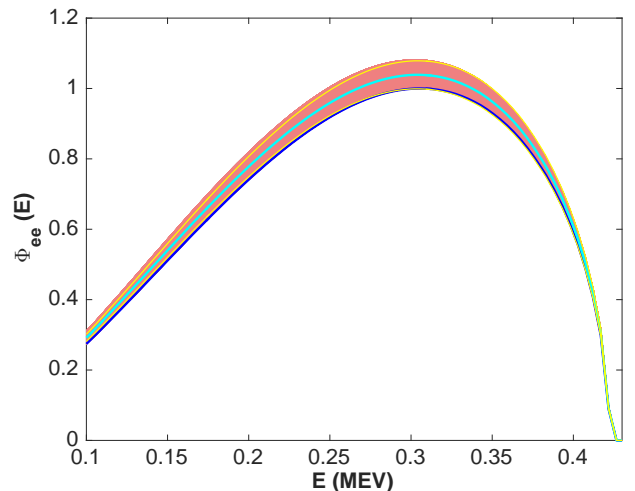


FIG. 6.— The pp solar electron neutrino spectra measured on Earth detectors. The LDM model and color scheme is the same one as in Figure 5. The error bar curves (yellow curves) on the averaged (distorted) electron spectra (cyan curve) corresponds to the expected precision to be attained by the Darwin experiment (Aalbers et al. 2020). See Figure 4 and main the text.

mass-square difference and the mixing angles have the following values: $\Delta m_{21}^2 = 7.50^{+0.22}_{-0.20} \times 10^{-5} \text{eV}^2$, $\sin^2 \theta_{12} = 0.318 \pm 0.016$, and $\sin^2 \theta_{13} = 0.02250^{+0.00055}_{-0.00078}$. Although, $\Delta m_{31}^2 = 2.56^{+0.0003}_{-0.0004} \times 10^{-3} \text{eV}^2$ and $\sin^2 \theta_{23} = 0.56^{+0.016}_{-0.022}$, we mention them here for reference (de Salas et al. 2020). These new parameters are consistent with previous estimations (Esteban et al. 2019; Gonzalez-Garcia et al. 2016). For the sterile neutrino, we choose the following fiducial values for the mass-square difference and mixing angles (Gariazzo et al. 2015, 2016; Capozzi et al. 2017): $\Delta m_{41}^2 = 1.6 \text{eV}^2$, $\sin^2 \theta_{14} = 0.027$, $\sin^2 \theta_{42} = 0.014$ and the other mixing angle for the sterile neutrinos are fixed to zero. Moreover, we assume that all phases ($\delta_{13,14,34}$) and other angles related to the sterile neutrino are equal to zero.

The present-day internal structure of the Sun corresponds to an up-to-date standard solar model (SSM) that has a better agreement with neutrino fluxes and helioseismic data sets. This solar model was obtained from a one-dimensional stellar evolution code allowed to evolve in time until the present-day solar age, 4.57 Gyr, having been calibrated to the values of luminosity and effective temperature of the present Sun, of $3.8418 \times 10^{33} \text{erg s}^{-1}$ and 5777 K, respectively, as well as the observed abundance ratio at the Sun's surface: $(Z_s/X_s)_\odot = 0.0181$, where Z_s and X_s are the metal and hydrogen abundances at the surface of the star (Turck-Chieze and Lopes 1993; Bahcall et al. 1995, 2006). This stellar model was computed with the release version 12115 of the stellar evolution code MESA (Paxton et al. 2011, 2019). The details about the physics of this standard solar model in which we use the AGSS09 (low-Z) solar abundances (Asplund et al. 2009) are described in Lopes and Silk (2013) and Capelo and Lopes (2020).

Figures 1 and 2 show the impact of the time-dependent mass-square difference (Equation 6) and mixing angles (Equation 7) on the averaged electron survival probability $\langle P_{ee}(E) \rangle$ (Equation 15) for which the LDM field ϕ has a fixed amplitude (Equation 5): $\epsilon_\phi = 0$ or $\epsilon_\phi = 1.5\%$. We also show LDM models for which the sterile neutrino couples to ϕ with strength G_ϕ .

The overall shape of the curve $\langle P_{ee}(E) \rangle$ depends on G_ϕ times

n_ϕ in the potential $V_{\nu_s\phi}$ or the ratio G_ϕ/m_ϕ as previously mentioned. For instance, in a LDM model in which we fix $m_\phi = 10^{-9}$ eV (or n_ϕ), an increase of G_ϕ from 10^{20} to 10^{22} G_F leads $\langle P_{ee}(E) \rangle$ to vary significantly, as shown in Figure 1. As expected this change in $\langle P_{ee}(E) \rangle$ is more pronounced for high energy neutrinos where the MSW effect is more significant. If we choose higher values of m_ϕ the results will somehow be similar (see Figure 1).

Evidently, for an LDM model in which m_ϕ decreases by a certain amount ($n_\phi = \rho_\phi/m_\phi$), the constancy of G_ϕ/m_ϕ in $V_{\nu_s\phi}$ implies that G_ϕ can increase by the same order of magnitude to obtain the same MSW effect on the $\langle P_{ee}(E) \rangle$ curve (see Figure 1). For instance, an LDM model with $m_\phi = 10^{-23}$ eV and $G_\phi = 10^7 G_F$ will have $\langle P_{ee}(E) \rangle$ identical to an LDM model with $m_\phi = 10^{-9}$ eV and $G_\phi = 10^{21} G_F$, since in both LDM models we have the same ratio: $G_\phi/m_\phi \approx 10^{30}$. The same argument explains the reason why the coupling constant between sterile neutrinos and more massive dark matter particles is much smaller in those models than in the present study. For instance, this is the case for particles captured from the dark matter halo by the Sun. Since over time, the star accreted a significant amount of dark matter (e.g., Lopes 2018a), for these models G_ϕ is significantly smaller than the value found for the present study.

The most important feature of such a class of LDM models is the time dependence of the dark matter field $\phi(t)$ and its imprint in the flavor oscillation parameters' mass-square differences (Equation 6) and mixing angles (Equation 7). As predicted by equation 9, there are many $P_{ee}(E, \phi)$ with near similar behavior. Figure 1 shows an ensemble of time-dependent $P_{ee}(E, \phi)$ as a pink band. The difference between curves relates to the dependence of the oscillation parameters on time. In this LDM model it is assumed there is a very negligible interaction between sterile neutrinos and ϕ (for which $G_\phi \approx 0$). The figure also shows $\langle P_{ee}(E) \rangle$ (red curve) the time-averaged of the ensemble of $P_{ee}(E, \phi)$ curves that we compute using equation 15.

Although there are several parameters that contribute for the time variability of $P_{ee}(E, \phi)$ (Equation 9), the main contributions come from θ_{21} and θ_{13} . The variability related θ_{24} is relevant for the high energies. We notice that the contributions coming from Δm_{21}^2 and θ_{32} are much smaller than all the parameters mentioned above. The amplitude of the $P_{ee}(E, \phi)$ pink band is defined by the value of ϵ_ϕ for which we adopt the fiducial value of $\epsilon_\phi = 1.5\%$. It is worth pointing out that the $P_{ee}(E, \phi)$ band is much larger for low-energy than for higher-energy values. Moreover, the averaged value of this ensemble given by $\langle P_{ee}(E) \rangle$ is identical to $\langle P_{ee}(E) \rangle$ with $\epsilon_\phi \approx 0$. Figure 2 shows the variability of $P_{ee}(E, \phi)$ for a LDM with different G_ϕ values. These results are identical to the model in figure 1. Nevertheless, the LDM model with the largest G_ϕ has (an orange) band with a smaller amplitude around $\langle P_{ee}(E) \rangle$. Once again, the band thickness decreases for neutrinos with higher energy for all these models.

Figures 3 and 4 compare our predictions with current solar neutrino data (e.g., Aalbers et al. 2020). These figures show that LDM models with relatively low values of ϵ_ϕ and G_ϕ are compatible overall with current solar neutrino data coming from Borexino, Super-Kamiokande, and SNO. Clearly, this analysis has also shown that the precision of our current solar neutrino experiments is not able to distinguish between some

of these LDM models. Nevertheless, it is already possible to put some constraints on these LDM models. For instance, we found that LDM models with $G_\phi \approx 0$ must have a ϵ_ϕ smaller than 3% to be consistent with all data, including pp measurements of the Borexino detector (Borexino Collaboration et al. 2020) (see Figure 3); and any LDM models must have a ratio G_ϕ/m_ϕ smaller than 10^{30} , otherwise they become inconsistent with pp and ${}^7\text{Be}$ measurements for several solar detectors (Borexino Collaboration et al. 2020; Agostini et al. 2019; Borexino Collaboration et al. 2018; Bellini et al. 2010) (see figure 4). Figure 4 shows a LDM model with a $m_\phi = 10^{-9}$ eV and $G_\phi = 10^{22}$ G_F with a ratio G_ϕ/m_ϕ of the order of 10^{31} G_F (see Figure 4); This ratio is one order of magnitude larger than the critical G_ϕ/m_ϕ value of 10^{30} discussed in the previous section. Figure 4 also shows that the variability related with time dependence on $P_{ee}(E, \phi)$ decreases for large values of G_ϕ .

There is another important effect that also contributes to the time variability of $P_{ee}(E, \phi)$. The PP chain and CNO cycle, nuclear reactions occur at different distances from the center of the Sun and each nuclear reaction emits neutrinos in a well-defined energy range. As a consequence, the electron neutrinos produced in each specific nuclear reaction will be affected differently by the MSW effect. As such, this effect will also contribute to the overall variability of electron neutrinos $P_{ee,i}(E, \phi)$ (see Equation 16) and their time-averaged $\langle P_{ee,i}(E, \phi) \rangle$ (see Equation 17).

The time-dependent electron neutrino survival probability will have a significant impact on the neutrino spectra of the different nuclear reactions. Accordingly, figures 5 and 6 show the spectra correspond to two neutrino types: pp and ${}^8\text{B}$ neutrinos. An essential difference between these two spectra relates to the thickness of the ϵ_ϕ band for a fixed value since thickness decreases with neutrino energy. Therefore the ϵ_ϕ band is more significant for a pp spectrum than for a ${}^8\text{B}$ neutrino spectrum. This is an effect identical to the one discussed previously for the $P_{ee}(E, \phi)$ functions. Therefore, the measurement of solar neutrino fluxes and solar neutrino spectrum in the energy range below 0.2 MeV will provide the strongest constraint for such a class of dark matter models. Figure 5 and 6 show the spectra of ${}^8\text{B}$ and pp, if we assume the precision expected to be attained by the Darwin experiment (Aalbers et al. 2020). Figure 6 also shows the precision expected for the Darwin experiment.

6. CONCLUSION

This article focuses on the impact of LDM on solar neutrino fluxes, spectra, and survival probabilities of electron neutrinos, specifically a dark matter model made of two particles: a sterile neutrino and an LDM particle. In particular, we describe how the 3+1 neutrino flavor model is affected by this type of LDM particles, with an emphasis on how the LDM affects the Wolfenstein potentials. We also study how the dark matter models affect the survival probability functions of electron neutrinos related to the different nuclear reactions occurring in the solar interior, and we compute the spectra of two relevant solar neutrino sources: pp and ${}^8\text{B}$ neutrino nuclear reactions.

By studying a large range of dark matter particle masses (from 10^{-9} to 10^{-23} eV) we found that depending on the mass of these LDM particles and the value of the generalized Fermi constant, the shape of electron neutrino survival

probability and their spectra can vary with time. We establish that for LDM particles with low masses (low-frequency regime), the solar neutrino detectors can observe the electron neutrino survival probability changing with time. Conversely, for dark matter particles with higher masses (high-frequency regime), this impact can be determined by measuring the time-averaged electron neutrino survival probability.

It was possible to establish, using data of current solar neutrino measurements, that those models with a G_ϕ/m_ϕ ratio smaller than $10^{30} G_F eV^{-1}$ agree with current solar neutrino data from the Borexino, SNO and Super-Kamiokande detectors. We also found that for models with a near-zero constant, the time-variability amplitude must be smaller than 3%. Such a constraint is equivalent to the condition

$$g_\phi \sqrt{2\rho_{DM}^\odot/(m_\phi m_\nu)} (\Omega_\phi/\Omega_{DM})^{1/2} \leq 0.03.$$

Finally, we also found that the precision expected in the measurements to be made by the Darwin detector will allow us to put powerful constraints to this class of models.

The author is grateful to the MESA team for having made their code publicly available. The author also thanks the anonymous referee for the revision of the manuscript. I.L. thanks the Fundação para a Ciência e Tecnologia (FCT), Portugal, for the financial support to the Center for Astrophysics and Gravitation (CENTRA/IST/ULisboa) through the Grant Project No. UIDB/00099/2020 and grant No. PTDC/FIS-AST/28920/2017.

REFERENCES

- Aalbers, J., and 166 colleagues 2020, "Solar Neutrino Detection Sensitivity in DARWIN via Electron Scattering", arXiv e-prints, arXiv:2006.03114.
- Abe, K., and 169 colleagues 2016, "Solar neutrino measurements in Super-Kamiokande-IV", *Phys. Rev. D*, 94, 052010.
- Adam, T., and 396 colleagues 2015, "JUNO Conceptual Design Report", arXiv e-prints, arXiv:1508.07166.
- Agostini, M., and 107 colleagues 2019, "Simultaneous precision spectroscopy of $p\bar{p}$, ${}^7\text{Be}$, and $p\bar{e}p$ solar neutrinos with Borexino Phase-II", *Phys. Rev. D*, 100, 082004.
- Aharmim, B., and 124 colleagues 2010, "Searches for High-frequency Variations in the ${}^8\text{B}$ Solar Neutrino Flux at the Sudbury Neutrino Observatory", *ApJ*, 710, 540-548.
- Aharmim, B., and 122 colleagues 2013, "Combined analysis of all three phases of solar neutrino data from the Sudbury Neutrino Observatory", *Phys. Rev. C*, 88, 025501.
- Aguiar, A., and 25 colleagues 2001, "Evidence for neutrino oscillations from the observation of $\bar{\nu}_e$ appearance in a $\bar{\nu}_\mu$ beam", *Phys. Rev. D*, 64, 112007.
- Arvanitaki, A., S. Dimopoulos, and K. Van Tilburg 2016, "Sound of Dark Matter: Searching for Light Scalars with Resonant-Mass Detectors", *Phys. Rev. Lett.*, 116, 031102.
- Arvanitaki, A., P. W. Graham, J. M. Hogan, S. Rajendran, and K. Van Tilburg 2018, "Search for light scalar dark matter with atomic gravitational wave detectors", *Phys. Rev. D*, 97, 075020.
- Asplund, M., N. Grevesse, A. J. Sauval, and P. Scott 2009, "The Chemical Composition of the Sun", *ARA&A*, 47, 481-522.
- An, F., and 227 colleagues 2016, "Neutrino physics with JUNO", *Journal of Physics G Nuclear Physics*, 43, 030401.
- Bahcall, J. N. and R. Davis 1976, "Solar Neutrinos: A Scientific Puzzle", *Science*, 191, 264-267.
- Bahcall, J. N., M. H. Pinsonneault, and G. J. Wasserburg 1995, "Solar models with helium and heavy-element diffusion", *Reviews of Modern Physics*, 67, 781-808.
- Bahcall, J. N., A. M. Serenelli, and S. Basu 2006, "10,000 Standard Solar Models: A Monte Carlo Simulation", *ApJS*, 165, 400-431.
- Bellini, G., and 86 colleagues 2010, "Measurement of the solar B8 neutrino rate with a liquid scintillator target and 3 MeV energy threshold in the Borexino detector", *Phys. Rev. D*, 82, 033006.
- Berlin, A. 2016, "Neutrino Oscillations as a Probe of Light Scalar Dark Matter", *Phys. Rev. Lett.*, 117, 231801.
- Bezrukov, F., A. Chudaykin, and D. Gorbunov 2019, "Induced resonance makes light sterile neutrino dark matter cool", *Phys. Rev. D*, 99, 083507.
- Bezrukov, F., A. Chudaykin, and D. Gorbunov 2020, "Scalar induced resonant sterile neutrino production in the early Universe", *Phys. Rev. D*, 101, 103516.
- Blas, D., D. L. Nacir, and S. Sibiryakov 2017, "Ultralight Dark Matter Resonates with Binary Pulsars", *Phys. Rev. Lett.*, 118, 261102.
- Blennow, M. and A. Y. Smirnov 2013, "Neutrino Propagation in Matter", arXiv e-prints, arXiv:1306.2903.
- Borexino Collaboration et al., Agostini, M., and 98 colleagues 2020, "Improved measurement of ${}^8\text{B}$ solar neutrinos with 1.5 kt.y of Borexino exposure", *Phys. Rev. D*, 101, article id.062001.
- Borexino Collaboration, M. Agostini, and 108 colleagues 2018, "Comprehensive measurement of pp-chain solar neutrinos", *Nature*, 562, 505-510.
- Brdar, V., J. Kopp, J. Liu, P. Prass, and X.-P. Wang 2018, "Fuzzy dark matter and nonstandard neutrino interactions", *Phys. Rev. D*, 97, 043001.
- Catena, R. and P. Ullio 2010, "A novel determination of the local dark matter density", *Journal of Cosmology and Astroparticle Physics*, 2010, 004.
- Capelo, D. and I. Lopes 2020, "The impact of composition choices on solar evolution: age, helio- and asteroseismology, and neutrinos", *MNRAS*, 498, 1992-2000.
- Capozzi, F., I. M. Shoemaker, and L. Vecchi 2017, "Solar neutrinos as a probe of dark matter-neutrino interactions", *Journal of Cosmology and Astroparticle Physics*, 2017, 021.
- Cravens, J. P., and 144 colleagues 2008, "Solar neutrino measurements in Super-Kamiokande-II", *Phys. Rev. D*, 78, 032002.
- Dasgupta, B. and J. Kopp 2014, "Cosmologically Safe eV-Scale Sterile Neutrinos and Improved Dark Matter Structure", *Phys. Rev. Lett.*, 112, 031803.
- de Gouvêa, A., M. Sen, W. Tangarife, and Y. Zhang 2020, "Dodelson-Widrow Mechanism in the Presence of Self-Interacting Neutrinos", *Phys. Rev. Lett.*, 124, 081802.
- Dev, A., P. A. N. Machado, and P. Martínez-Miravé 2020, "Signatures of Ultralight Dark Matter in Neutrino Oscillation Experiments", arXiv e-prints, arXiv:2007.03590.
- de Salas, P. F., D. V. Forero, S. Gariazzo, P. Martínez-Miravé, O. Mena, C. A. Ternes, M. Tórtola, and J. W. F. Valle 2020, "2020 Global reassessment of the neutrino oscillation picture", arXiv e-prints, arXiv:2006.11237.
- Diaz, A., C. A. Argüelles, G. H. Collin, J. M. Conrad, and M. H. Shaevitz 2019, "Where Are We With Light Sterile Neutrinos?", arXiv e-prints, arXiv:1906.00045.
- Ding, G.-J., F. Feruglio Testing Moduli and Flavon Dynamics with Neutrino Oscillations, arXiv e-prints, arXiv:2003.13448.
- Dodelson, S. and L. M. Widrow 1994, "Sterile neutrinos as dark matter", *Phys. Rev. Lett.*, 72, 17-20.
- Dror, J. A., K. Harigaya, and V. Narayan 2019, "Parametric resonance production of ultralight vector dark matter", *Phys. Rev. D*, 99, 035036.
- DUNE Collaboration, R. Acciarri, and 804 colleagues 2015, "Long-Baseline Neutrino Facility (LBNF) and Deep Underground Neutrino Experiment (DUNE) Conceptual Design Report Volume 2: The Physics Program for DUNE at LBNF", arXiv e-prints, arXiv:1512.06148.
- Esteban, I., M. C. Gonzalez-Garcia, A. Hernandez-Cabezudo, M. Maltoni, and T. Schwetz 2019, "Global analysis of three-flavour neutrino oscillations: synergies and tensions in the determination of θ_{23} , δ_{CP} , and the mass ordering", *Journal of High Energy Physics*, 2019, 106.
- Farzan, Y. 2019, "Ultra-light scalar saving the 3 + 1 neutrino scheme from the cosmological bounds", *Physics Letters B*, 797, 134911.
- Graham, P. W., D. E. Kaplan, J. Mardon, S. Rajendran, and W. A. Terrano 2016, "Dark matter direct detection with accelerometers", *Phys. Rev. D*, 93, 075029.
- Gariazzo, S., C. Giunti, M. Laveder, Y. F. Li, and E. M. Zavatin 2016, "Light sterile neutrinos", *Journal of Physics G Nuclear Physics*, 43, 033001.

- Gariazzo, S., C. Giunti, M. Laveder, Y. F. Li, and E. M. Zavatin 2015, "Light sterile neutrinos", *Journal of Physics G Nuclear Physics*, 43, 033001.
- Gonzalez-Garcia, M. C., M. Maltoni, and T. Schwetz 2016, "Global analyses of neutrino oscillation experiments", *Nuclear Physics B*, 908, 199-217.
- Giunti, C. and Y. F. Li 2009, "Matter effects in active-sterile solar neutrino oscillations", *Phys. Rev. D*, 80, 113007.
- Giunti, C., M. Laveder, Y. F. Li, Q. Y. Liu, and H. W. Long 2012, "Update of short-baseline electron neutrino and antineutrino disappearance", *Phys. Rev. D*, 86, 113014.
- Giunti, C., M. Laveder, Y. F. Li, and H. W. Long 2013, "Short-baseline electron neutrino oscillation length after the Troitsk experiment", *Phys. Rev. D*, 87, 013004.
- Hannestad, S., R. S. Hansen, and T. Tram 2014, "How Self-Interactions can Reconcile Sterile Neutrinos with Cosmology", *Phys. Rev. Lett.*, 112, 031802.
- Hu, W., R. Barkana, and A. Gruzinov 2000, "Fuzzy Cold Dark Matter: The Wave Properties of Ultralight Particles", *Phys. Rev. Lett.*, 85, 1158-1161.
- Hui, L., J. P. Ostriker, S. Tremaine, and E. Witten 2017, "Ultralight scalars as cosmological dark matter", *Phys. Rev. D*, 95, 043541.
- Khmelnitsky, A. and V. Rubakov 2014, "Pulsar timing signal from ultralight scalar dark matter", *Journal of Cosmology and Astroparticle Physics*, 2014, 019.
- Krnjaic, G., P. A. N. Machado, and L. Necib 2018, "Distorted neutrino oscillations from time varying cosmic fields", *Phys. Rev. D*, 97, 075017.
- Kuo, T. K. and J. Pantaleone 1986, "Solar-neutrino problem and three-neutrino oscillations.", *Phys. Rev. Lett.*, 57, 1805-1808.
- Lopes, I. 2013, "Probing the Sun's inner core using solar neutrinos: A new diagnostic method", *Phys. Rev. D*, 88, 045006.
- Lopes, I. 2017, "New neutrino physics and the altered shapes of solar neutrino spectra", *Phys. Rev. D*, 95, 015023.
- Lopes, I. 2018, "The Sterile-Active Neutrino Flavor Model: The Imprint of Dark Matter on the Electron Neutrino Spectra", *ApJ*, 869, 112.
- Lopes, I. 2018, "The spectroscopy of solar sterile neutrinos", *European Physical Journal C*, 78, 327.
- Lopes, J. and I. Lopes 2019, "Asymmetric Dark Matter Imprint on Low-mass Main-sequence Stars in the Milky Way Nuclear Star Cluster", *ApJ*, 879, 50.
- Lopes, I. and J. Silk 2019, "Dark matter imprint on ^8B neutrino spectrum", *Phys. Rev. D*, 99, 023008.
- Lopes, I. and J. Silk 2014, "Helioseismology and Asteroseismology: Looking for Gravitational Waves in Acoustic Oscillations", *ApJ*, 794, 32.
- Lopes, I. and S. Turck-Chièze 2013, "Solar Neutrino Physics Oscillations: Sensitivity to the Electronic Density in the Sun's Core", *ApJ*, 765, 14.
- Lopes, I. and J. Silk 2013, "Planetary influence on the young Sun's evolution: the solar neutrino probe", *MNRAS*, 435, 2109-2115.
- Lunardini, C. and A. Y. Smirnov 2000, "The minimum width condition for neutrino conversion in matter", *Nuclear Physics B*, 583, 260-290.
- Kuo, T. K. and J. Pantaleone 1989, "Neutrino oscillations in matter", *Reviews of Modern Physics*, 61, 937-980.
- Kostensalo, J., J. Suhonen, C. Giunti, and P. C. Srivastava 2019, "The gallium anomaly revisited", *Physics Letters B*, 795, 542-547.
- Kusenko, A. 2009, "Sterile neutrinos: The dark side of the light fermions", *Phys. Rep.*, 481, 1-28.
- Maltoni, M. and A. Y. Smirnov 2016, "Solar neutrinos and neutrino physics", *European Physical Journal A*, 52, 87.
- Mikheyev, S. P. and A. Y. Smirnov 1985, "Resonance enhancement of oscillations in matter and solar neutrino spectroscopy", *Yadernaya Fizika*, 42, 1441-1448.
- MiniBooNE Collaboration, A. A. Aguilar-Arevalo, and 47 colleagues 2018, arXiv e-prints, arXiv:1805.12028.
- Miranda, O. G., C. A. Moura, and A. Parada 2015, "Sterile neutrinos, dark matter, and resonant effects in ultra high energy regimes", *Physics Letters B*, 744, 55-58.
- Mocz, P., and 12 colleagues 2019, "First Star-Forming Structures in Fuzzy Cosmic Filaments", *Phys. Rev. Lett.*, 123, 141301.
- Niemeyer, J. C. 2019, "Small-scale structure of fuzzy and axion-like dark matter", arXiv e-prints, arXiv:1912.07064.
- Palazzo, A. 2011, "Testing the very-short-baseline neutrino anomalies at the solar sector", *Phys. Rev. D*, 83, 113013.
- Paxton, B., L. Bildsten, A. Dotter, F. Herwig, P. Lesaffre, and F. Timmes 2011, "Modules for Experiments in Stellar Astrophysics (MESA)", *ApJS*, 192, 3.
- Paxton, B., and 16 colleagues 2019, "Modules for Experiments in Stellar Astrophysics (MESA): Pulsating Variable Stars, Rotation, Convective Boundaries, and Energy Conservation", *ApJS*, 243, 10.
- Planck Collaboration, N. Aghanim, and 181 colleagues 2018, "Planck 2018 results. VI. Cosmological parameters", arXiv e-prints, arXiv:1807.06209.
- Peebles, P. J. E. 2000, "Fluid Dark Matter", *ApJ*, 534, L127-L129.
- Primack, J. R. 2009, "Cosmology: small-scale issues", *New Journal of Physics*, 11, 105029.
- Smirnov, A. Y. and X.-J. Xu 2019, "Wolfenstein potentials for neutrinos induced by ultra-light mediators", *Journal of High Energy Physics*, 2019, 46.
- Shi, X. and G. M. Fuller 1999, "New Dark Matter Candidate: Nonthermal Sterile Neutrinos", *Phys. Rev. Lett.*, 82, 2832-2835.
- Turck-Chieze, S. and I. Lopes 1993, "Toward a Unified Classical Model of the Sun: On the Sensitivity of Neutrinos and Helioseismology to the Microscopic Physics", *ApJ*, 408, 347.
- Wang, B., E. Abdalla, F. Atrio-Barandela, and D. Pavón 2016, "Dark matter and dark energy interactions: theoretical challenges, cosmological implications and observational signatures", *Reports on Progress in Physics*, 79, 096901.
- Wolfenstein, L. 1978, "Neutrino oscillations in matter", *Phys. Rev. D*, 17, 2369-2374.
- Yoo, J., and 130 colleagues 2003, "Search for periodic modulations of the solar neutrino flux in Super-Kamiokande-I", *Phys. Rev. D*, 68, 092002.
- Xing, Z.-zhong . 2020, "Flavor structures of charged fermions and massive neutrinos", *Phys. Rep.*, 854, 1-147.